

Unambiguous joint detection of spatially separated properties of a single photon in the two arms of an interferometer

Surya Narayan Sahoo,¹ Sanchari Chakraborti,¹ Som Kanjilal,²

Dipankar Home,² Alex Matzkin,³ and Urbasi Sinha^{1,*}

¹*Light and Matter Physics, Raman Research Institute, Bengaluru 560080, India*

²*Center for Astroparticle Physics and Space Science (CAPSS),
Bose Institute, Kolkata 700 091, India*

³*Laboratoire de Physique Théorique et Modélisation,
CNRS Unité 8089, CY Cergy Paris Université,
95302 Cergy-Pontoise cedex, France*

Abstract

The quantum superposition principle implies that a particle entering an interferometer evolves by simultaneously taking both arms. If a non-destructive, minimally-disturbing interaction coupling a particle property to a pointer is implemented on each arm while maintaining the path superposition, quantum theory predicts that, for a fixed state measured at the output port, certain particle properties can be associated with only one or the other path. Here we report realization of this prediction through joint observation of the spatial and polarization degrees of freedom of a single photon in the two arms of an interferometer. Significant pointer shifts (~ 50 microns) are observed in each arm. This observation, involving coupling distinct properties of a quantum system in spatially separated regions, opens new possibilities for quantum information protocols and for tests of quantumness for mesoscopic systems.

*Electronic address: usinha@rri.res.in

Manifestations of the quantum superposition of states in a two-arm interferometer open avenues for empirically probing intriguing questions, such as whether it is possible to jointly detect signatures of distinct particle properties in different arms of an interferometer. Indeed, a quantum particle, say a single photon entering an interferometer is said to travel along both arms simultaneously (1). This is generally evidenced by monitoring the resulting interference at the exit port. Instead, if a measurement is made earlier on one or the other arm, the photon will be detected on that arm with some probability and the interference pattern will disappear. Modifying an interaction at an intermediate time, such as removing the exit beam-splitter once the photon is already inside the interferometer in the famous delayed-choice experiment (2) changes the observed properties of the photon. More generally, an intermediate non-destructive measurement of a given observable can be made on one of the arms and the photon is then measured at the exit port and filtered to a chosen final state (3). The photon will then be found to have a given value of the measured property on that arm, with a probability conditioned by the final state (as confirmed by a recent experiment (4)). For certain observables like projectors giving a yes/no answer, an intermediate outcome “yes” can be obtained with a unit conditional probability on a given arm, say arm A (and consequently zero probability on the other arm B). Therefore the particle will always be found with the property associated with that observable on arm A, never on the other. However, if a different observable is measured, the particle will sometimes be found (in an eigenstate of the measured observable) on arm B.

Consider a single photon entering the Mach-Zehnder interferometer (MZI) of Figure 1. We prepare the state after the beam-splitter BS1 to be $|\psi\rangle = \frac{1}{\sqrt{2}}(|A\rangle|H\rangle + |B\rangle|V\rangle)$, where $|A\rangle$ and $|B\rangle$ denote the spatial wavefunctions in arms A and B respectively; this preparation procedure (2) is known as “pre-selection”. When detecting the photon at the exit port, we filter the measured state keeping only the outcomes corresponding to $|\phi\rangle = \frac{1}{\sqrt{2}}(|A\rangle + |B\rangle)|H\rangle$. This filtering procedure is known as “post-selection”. Let $\hat{Y}_i = |i\rangle\langle i| \otimes \hat{\mathbb{I}}$ represent the spatial projection operator on arm $i = A, B$ and let $\hat{X}_i = |i\rangle\langle i| \otimes \hat{\sigma}_1$ represent a diagonal polarization measurement on arm i (σ_1 is a Pauli matrix). The probability for the photon to be found on arm A (conditioned on successful post-selection of $|\phi\rangle$) is given by $P(Y_A = 1|\phi) = 1$, and therefore on arm B $P(Y_B = 1|\phi) = 0$ ($Y_i = 0, 1$ denotes the eigenvalues of \hat{Y}_i): a non-destructive intermediate measurement of the position degree of freedom will always find the photon on arm A (5). However, if the photon polarization in

the diagonal basis $\{|\nearrow\rangle, |\searrow\rangle\}$ on a particular path i i.e., \hat{X}_i is measured, instead of the position, there is a non-zero probability to find a photon on arm B with diagonal $|\nearrow\rangle$ or anti-diagonal $|\searrow\rangle$ polarization. One can further specifically couple \hat{X}_i to a qubit pointer whose excited state detects a quantity we may call the “net diagonal polarization” (defined for an arbitrary state $\alpha|\nearrow\rangle + \beta|\searrow\rangle$ by $|\alpha - \beta|^2$ (5)); such a pointer could be found excited on arm B, never on arm A. Hence with our choices of pre and post-selected states, a pointer “triggers” (for example, its position shifts) only on arm A if the spatial degree of freedom is measured, but on arm B if a different property like the diagonal component of polarization degree of freedom is measured. There is nevertheless no paradox: Bohr (6) and Wheeler (7) proscribed long ago the use of counterfactual reasoning while attempting to account for the behavior of quantum systems measured under different experimental conditions within a single picture. The reason is that measurements disturb the system. Indeed if only \hat{Y}_A is measured, the photon will always be found on arm A, but if only \hat{X}_B is measured it is not possible to ascribe a property to the spatial position of the same photon on arm A had \hat{Y}_A been measured. When $\{\hat{X}_B, \hat{Y}_A\}$ are measured jointly, the system coherence is disturbed, and we will obtain with equal probabilities either the photon position on arm A or the photon’s diagonal polarization on arm B.

In order to keep the coherence essentially intact while jointly detecting the spatially separated properties on each arm for a single photon in the same run of the experiment, minimally disturbing intermediate interactions need to be implemented. This is the objective of our experiment whose results are reported below. For this purpose, we use what are known as weak measurements (8) wherein very weak couplings are combined with pre and post-selected states (as defined in Figure 1). In this situation, the shift of a pointer weakly coupled to a system observable \hat{S} is proportional to the real part of a quantity known as the weak value $S^w = \langle\phi|\hat{S}|\psi\rangle / \langle\phi|\psi\rangle$. In the present setup, with the notation introduced previously, it follows that $Y_A^w = 1, X_B^w = 1$. These weak values imply the following key feature: the pointer that is weakly coupled to the spatial degrees of freedom (DOF) on arm A and the pointer that is weakly coupled to the diagonal polarization DOF on arm B, both shift when a single photon passes through the interferometer. In addition, a logical consequence (see Appdx B) of having these weak values equal to unity is that $Y_B^w = 0$ and $X_A^w = 0$, so that weakly coupling the spatial DOF on arm B or the diagonal polarization DOF on arm A has no effect on the respective pointers. Thus, the pointers’ motions resulting from the weak

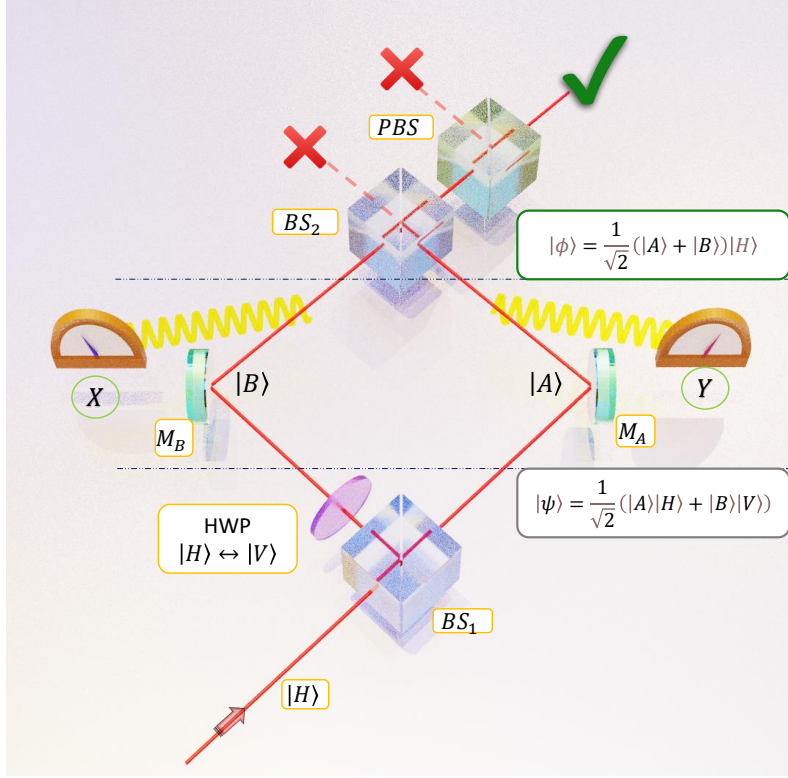


FIG. 1: Pre and post selection in a Mach Zehnder Interferometer. The observables \hat{X} and \hat{Y} are coupled to the pointers at an intermediate time between pre-selection with state $|\psi\rangle$ and post-selection with state $|\phi\rangle$.

couplings can be interpreted as reflecting the superposition of these two different photon properties along spatially separated arms. The spatial separation of the position degree of freedom from another property has amusingly been coined (9) the “Quantum Cheshire Cat” (QCC).

Genuine weak measurements are generally delicate to implement experimentally given that the coupling is weak and the experimentally measured quantities are often of the same order of magnitude as the experimental errors for certain choices of pre and post-selection. Several experiments in the last 15 years have measured weak values and their ramifications (10-16). Very often however, weak values are inferred by combining distinct projective (strong coupling) measurements. This has been the case in particular for past interferometric experiments dealing with the QCC, in which the weak values were computed from the difference in the intensities obtained employing set-ups with different experimental arrangements, as opposed to measurements of pointer shifts arising from minimally disturbing

interactions. In several experiments (17-19) such intensity differences were obtained employing set ups with or without absorbers present, and polarization or spin rotators inserted. A more recent work reconstructed weak values from pointer shifts by interpolating from results obtained using different interaction strengths (20). However, such methods preclude the joint observation of different properties in the same run (21). In order to observe the superposition of spatially separated properties, it is crucial to implement non-destructive minimally perturbing measurements on the same quantum particle along both arms.

In this work, employing the experimental architecture shown in Figure 2 with a single photon source, we perform joint weak measurements of \hat{Y}_A , the spatial DOF of the photon in arm A, and of \hat{X}_B , the diagonal component of polarisation DOF in arm B, in the same run of the experiment i.e. without any change in experimental settings between pre and post-selection. The photon is prepared in the pre-selected state $|\psi\rangle$ and weakly interacts with the optical elements associated with the observables to be measured inside the interferometer. The centre of the transverse spatial profile of the photon is used as the pointer. For the interaction involving the spatial DOF, we use a tilted glass plate that causes a vertical shift of the beam. The coupling of \hat{X}_B is made with two beam displacers that cause a horizontal shift in the pointer after the post-selection. A polarizing beam-splitter at the output port post-selects the photon to the state $|\phi\rangle$. Finally, the pointers' vertical and horizontal shifts are measured. Each step of the experiment is detailed in the Appdx A.

Being an interferometric experiment, steps have been taken to ensure maximum coherence as well as proper phase stabilization. One of the key features that we need to ensure in order to enable an unambiguous joint measurement is perfect overlap of the beams from the individual arms in the absence of the desired weak interaction. This involves a critical alignment procedure involving measuring the undeviated beam positions, while including all necessary interaction components. We also need to ascertain the values of the exact pointer shifts in microns for both weak interactions that would correspond to a weak value of 1, requiring further calibration (5). Ensuring coherence and maximum visibility requires prior alignment with a pulsed laser and a beam profiler camera before moving on to the heralded photon source. The signal photon passes through the interferometric set-up while the photon in the heralding arm is used to enable the measurement of coincidences at the desired pre and post selection conditions. A crucial requirement in our experiment is to ensure that

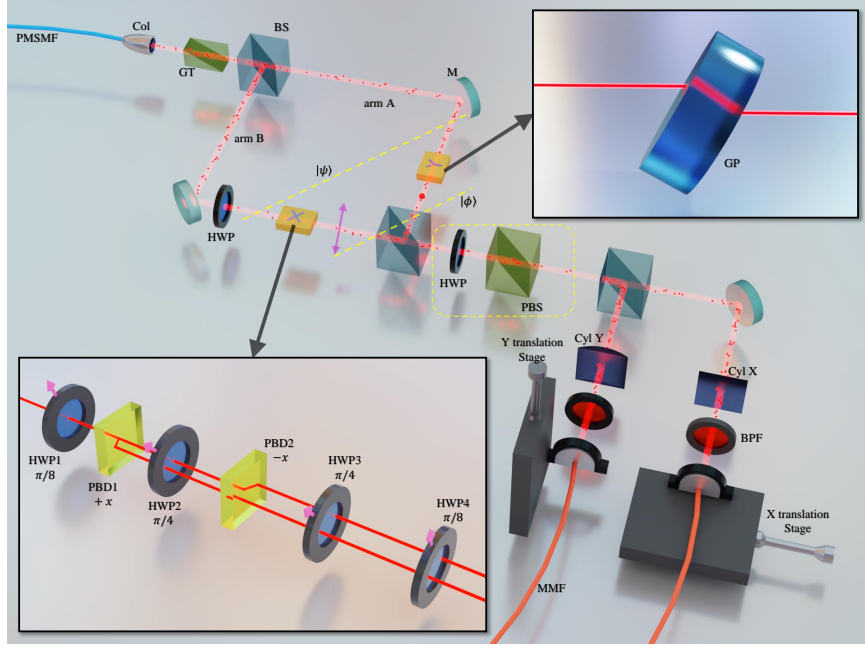


FIG. 2: Experimental schematic shows the MZI with pre and post-selection. The angle of the post-selection half wave plate (HWP) is kept at zero degree. In arm B, the apparatus to measure the σ_1 polarization component is inserted, which displaces the beam along the horizontal (X). The glass plate (GP) in arm A makes the beam shift vertically (along Y). A 50:50 beam-splitter placed after the polarising beam splitter (PBS) causes the photons to randomly make their way to two multi-mode fibres (MMF). One of the fibres is moved along X to generate the horizontal profile, after the beam passes through a cylindrical lens that compresses the vertical transverse profile. The other MMF is moved along Y to generate the vertical profile, after the horizontal transverse profile of the beam is compressed using another cylindrical lens. These two interactions simultaneously occur and no setting is changed between pre and post selection during the data acquisition, thus enabling joint weak measurement of the two observables \hat{X} and \hat{Y} .

we are performing joint measurements on the same photon. The use of heralded photons in our experiment ensures the same. We also show a measurement of cross correlation (g_2 measurement) in Appdx A to further substantiate the fulfillment of this requirement.

We show a representative result from our experiment in Figure 3. The figure demonstrates the histogram of weak values obtained for X^w (component of polarisation DOF) and Y^w (spatial DOF) measured jointly for the prepared pre and post selected states given above. Experimentally we reconstruct the transverse profile of the beam along the horizontal (X)

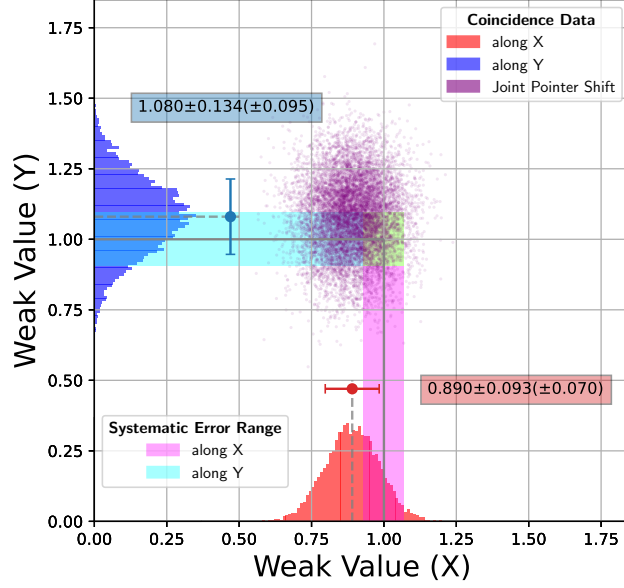


FIG. 3: The coincidence distribution of the photons for X^w is shown on the X axis through the red histogram plot. The mean and 1σ errors from the distribution are shown above the histogram while the values are mentioned alongside in the box. Similarly, the distribution for Y^w is shown along the Y-axis through the blue histogram plot. Since both the pointer shifts occur concurrently and are measured jointly in the experiment (i.e., without changing anything between pre and post-selection), the overall shift of the pointer would be along the diagonal as inferred from the shifts on the projections along horizontal X and vertical Y. The distribution of these diagonal shifts, in terms of the weak values, are represented by the scatter plots. The pink and light blue bands represent the systematic error bands for the coincidence measurements (± 0.070 for X^w and ± 0.095 for Y^w respectively). As can be seen, both measured weak values (0.890 ± 0.093 for X^w and 1.080 ± 0.134 for Y^w) lie well within the systematic error band of the experiment. Details of the error analysis are given in Appdx A.

and vertical (Y) directions as mentioned in Figure 2 and measure the pointer shifts associated with the two interactions \hat{X}_B and \hat{Y}_A from the positions of the centres of the respective profiles. From 10^4 such profile reconstructions we obtain the pointer shift along X to be $53.468 \pm 5.592 \mu m$ and the pointer shift along Y to be $56.809 \pm 7.026 \mu m$, where the values represent the mean $\pm 1\sigma$ error respectively. The weak values are then evaluated from the respective pointer shifts; we obtain X^w to be 0.89 ± 0.09 and Y^w to be 1.08 ± 0.13 respectively, along with attendant systematic error bands as shown in Figure 3. The

systematic error range estimates the drift in scale with respect to which the weak values are computed. This is primarily caused by beam pointing fluctuations as well as the drift in the centre of the beam due to acoustic and thermal response of the optomechanical components. Details of our data acquisition statistics as well as detailed error analysis (both statistical as well as systematic errors) are discussed in Appdx A.

These results are, to our knowledge, the first direct joint measurement of the weak values of different observables of a single quantum particle in distinct spatial regions. We have experimentally shown that a quantum pointer on one arm of the interferometer detects the spatial DOF of a photon in the chosen pre and post-selected states; at the same time, a pointer in the other arm detects the diagonal component of polarization DOF of the same photon. Our approach could pave the way to develop technologies implementing distinct interactions with different degrees of freedom of the same quantum system in different spatial regions, with minimal mutual perturbations. It should be worth exploring the application of the techniques used in our photonic experiment for demonstrating similar effects in massive particles by relying on the currently developing coherent atom-chip Stern-Gerlach interferometry (22) and thereby demonstrate the effect similar to the one shown in our photonic experiment. This could provide a potentially interesting dimension to the studies aiming to test the applicability of fundamental quantum features related to this work in the macroscopic regime. Our scheme could also be applied to quantum information protocols, for instance, to share the state of a qubit among spatially separated parties; a procedure for counterfactual quantum communication based on the Quantum Cheshire Cat effect was proposed very recently (23). Finally, we would like to conclude by raising the following provocative question: by going beyond Bohr's dictum (24) that we have no right to speak about what a photon does within an interferometer, can the effect shown in our experiment be interpreted as refining Bohr's principle of wave-particle complementarity? This is motivated by noting that in this experiment, the observables corresponding to particle-like properties of a single photon within each arm of the interferometer seemingly exhibit a wave-like superposition inside the interferometer. Of course, such a question needs to be formulated more precisely and revealing its full conceptual import could be a stimulating line of future study.

Acknowledgments

US acknowledges partial support provided by the Ministry of Electronics and Information Technology (MeitY), Government of India under grant for Centre for Excellence in Quantum Technologies with Ref. No. 4(7)/2020 – ITEA and QuEST-DST project Q-97 of the Govt. of India. DH and US would like to acknowledge partial support from the DST-ITPAR grant IMT/Italy/ITPAR-IV/QP/2018/G. DH also acknowledges support from the NASI Senior Scientist fellowship. We thank R. Chatterjee, S. Chatterjee, K. Joarder, Meena MS and Hafsa Syed for technical assistance.

References

1. J. A. Wheeler, in Quantum Theory and Measurement, J. A. Wheeler, W. H. Zurek, Eds. (Princeton Univ. Press, Princeton, NJ, 1984), pp. 182–200.
2. V. Jacques et al, Experimental realization of Wheeler’s delayed-choice gedanken experiment. *Science* 315, 966 (2007).
3. Y. Aharonov, P. G. Bergmann, and J. L. Lebowitz, Time Symmetry in the Quantum Process of Measurement, *Phys. Rev.* 134, B1410 (1964).
4. R. E. George et al, Classically undetectable wavefunction collapse, *PNAS* 110 (10) 3777-3781 (2013).
5. See Appendix.
6. N. Bohr, On the notions of causality and complementarity, *Dialectica*, 2: 312-319 (1948).
7. J. A. Wheeler, How Come the Quantum?, *Annals of the New York Academy of Sciences*, 480: 304-31 (1986).
8. Y. Aharonov, D. Z. Albert, and L. Vaidman, How the result of a measurement of a component of the spin of a spin-1/2 particle can turn out to be 100, *Phys. Rev. Lett.* 60, 1351 (1988).

9. Y. Aharonov *et al*, Quantum Cheshire Cats, *New J. Phys.* 15 113015 (2013).
10. G. J. Pryde *et al*, Measurement of Quantum Weak Values of Photon Polarization, *Phys. Rev. Lett.* 94, 220405 (2005).
11. O. Hosten and P. Kwiat, Observation of the Spin Hall Effect of Light via Weak Measurements, *Vol 319, Issue 5864*, pp. 787-790 (2008).
12. S. Kocsis *et al*, Observing the Average Trajectories of Single Photons in a Two-Slit Interferometer, *Science*, Vol 332, Issue 6034, pp. 1170-1173 (2011).
13. J. S. Lundeen *et al*, Direct measurement of the quantum wavefunction, *Nature* 474, 188–191 (2011).
14. G. Nirala *et al*, Measuring average of non-Hermitian operator with weak value in a Mach-Zehnder interferometer, *Phys. Rev. A* 99, 022111 (2019).
15. R. Ramos *et al.* Measurement of the time spent by a tunnelling atom within the barrier region. *Nature* 583, 529–532 (2020).
16. Y. Pan *et al.* Weak-to-strong transition of quantum measurement in a trapped-ion system. *Nat. Phys.* 16, 1206–1210 (2020).
17. T. Denkmayr *et.al.*, Observation of a quantum Cheshire Cat in a matter-wave interferometer experiment, *Nature Communications*, vol. 5, 4492 (2014).
18. D. P. Atherton, G. Ranjit, A. A. Geraci and J. D. Weinstein, Observation of a classical Cheshire cat in an optical interferometer, *Optics Letters*, vol. 40, no. 6, pp. 879-881, (2015).
19. J. M. Ashby, P. D. Schwarz and M. Schlosshauer, Observation of the quantum paradox of separation of a single photon from one of its properties, *Phys. Rev. A*, vol. 94, p. 012102, (2016).
20. Y. Kim *et. al*, Observing the quantum Cheshire cat effect with noninvasive weak measurement, *NPJ Quantum Information*, vol. 7, 13 (2021).
21. Q. Duprey *et al*, The Quantum Cheshire Cat effect: Theoretical basis and observational implications, *Annals of Physics*, vol. 391, pp. 1-15, (2018).

22. Y. Margalit et al, Realization of a complete Stern-Gerlach interferometer: Toward a test of quantum gravity, *Sci. Adv.* 7, 22, eabg2879 (2021).
23. Y. Aharonov, E. Cohen and S. Popescu, *Nature Comm.*, vol. 12, p. 4770, (2021).
24. N. Bohr, in *Albert Einstein: Philosopher-Scientist*, ed. P. A. Schilpp (Library of Living Philosophers, 1951) p. 230.

Appendix A: Experimental Details

1. Experimental Architecture

Setting up the Mach-Zehnder interferometer

The schematic of the experimental setup is given in Figure A-1. The stream of single photons of wavelength 810 nm (bandwidth about 2 nm) is made incident on the Mach Zehnder Interferometer (MZI) from a polarization maintaining single mode fibre PMSMF_s [PM780-HP, Thorlabs] to minimize pointing fluctuations of the beam. A suitable collimating lens COL [F240FC-780, Thorlabs] is used to get a beam size of about 1.5 mm and minimize divergence. The beam is passed through a Glan-Thompson polarizer GT [GTH5-B, Thorlabs] to ensure the polarization is horizontal with a high degree of purity before entering the 50:50 beam splitter BS_1 [BS014, Thorlabs]. In order to ensure that the path difference between the two arms of the MZI is negligible compared to the coherence length of the stream of detected photons, we use a corner cube retroreflector CCR [PS976M-B, Thorlabs] mounted on an actuator [ZST225-B, Thorlabs] attached to a 3D translation stage in one of the arms (here in arm B). The actuator is adjusted so that the path difference is ensured to be within ~ 2 microns. The CCR is used instead of a mirror assembly to avoid angular beam deviation upon translation. The CCR is attached to a piezo (osi-stack) which is used to stabilize the phase difference between the two arms of the MZI described later. However, since the CCR itself creates an additional path difference, this is macroscopically compensated using the three mirrors M_{T_1} , M_{T_2} and M_{T_3} [NIR 5102, Newport] in the A arm of the MZI. The CCR, however, introduces ellipticity in the polarization of the beam in arm B. This is corrected using a half-wave plate HWP_c [WPA03-H-810, Newlight Photonics] followed by quarter-wave plate QWP_c [WPA03-Q-810, Newlight Photonics] and the polarization is made vertical. An additional polarizing beam splitter PBS_T is introduced after the three mirrors in arm A to further purify the polarization. The second beam splitter BS_2 [BS014, Thorlabs] is fixed at the intersection point of the two beams and oriented to roughly ensure collinearity of the MZI. For fine alignment, the tip tilt degrees of freedom of the mirror mounts are used to ensure collinearity and the overlap of the beams is ensured by translation of the CCR. The overlap of beams is ensured down to 5 microns (although the precision of measuring the centre is much higher, at 0.1 microns, the spatial noise in the beam limits the accuracy) and the

angle between the two beams emerging out of the second beam splitter (BS_2) is ensured to be less than 10^{-5} radians (the actual value may be around 10^{-7} radians as estimated from the fringe stability of the interferometer). A half wave plate $HW P_{post}$ [WPZ0-200-L/2-810, Casteck] mounted in a motorized rotation mount [PRM1/MZ8, Thorlabs] is placed before a polarising beam splitter (PBS_{post} at one of the exit ports of the second beam splitter (BS_2). The post selected state changes with the change in the angle of $HW P_{post}$. In addition to the angle of interest, two more post selection angles are chosen to measure the reference pointer positions associated with the eigen values 0 and 1 respectively. This enables evaluating the weak value for a particular post selection from the measured pointer shift.

Pre- and post-selection

The pre-selected state is prepared after the compensating waveplate QWP_c on arm B and after PBS_T in arm A as depicted in Figure A-1. The post-selected state is obtained by back evolving the transmitted component of the post-selection PBS (PBS_{post}) to a time before the second beam splitter BS_2 of the MZI. Such a state, which is thus guaranteed to be transmitted in the PBS_{post} , is given by $|\phi(\theta)\rangle = \frac{1}{\sqrt{2}}(|A\rangle + |B\rangle) \otimes S(\theta)|H\rangle$. Here $S(\theta)$ is the Jones matrix for the HWP whose fast-axis is orientated at an angle θ from the horizontal in the post selection.

Ensuring Coherence

A band pass filter $BP10$ [FB810-10] followed by another $BP3$ [LL01-810-25] are used after PBS_{post} to prevent light of other wavelengths from being detected and also to narrow the linewidth down to at most 3 nm. The bandwidth of the filter determines the minimum coherence length. Visibility of the interference upon a suitable (diagonal, at $\theta = 22.5^\circ$) polarization post-selection is measured as a function of the path length difference by moving the actuator on which the CCR is mounted. Finally, the actuator is left at the position where maximum visibility is obtained.

Phase Stabilization

The relative phase between the two arms of the interferometer can drift due to mechanical and acoustic vibrations and therefore the CCR needs to be moved accordingly in order to maintain a constant phase relationship between the two arms. This is achieved by using the piezo (attached to the CCR) which contracts or expands depending on the voltage provided to it, thus causing the CCR to move. For this, a PID algorithm is implemented on a computer along with a DAQ card [USB-6003] which is used to generate and receive

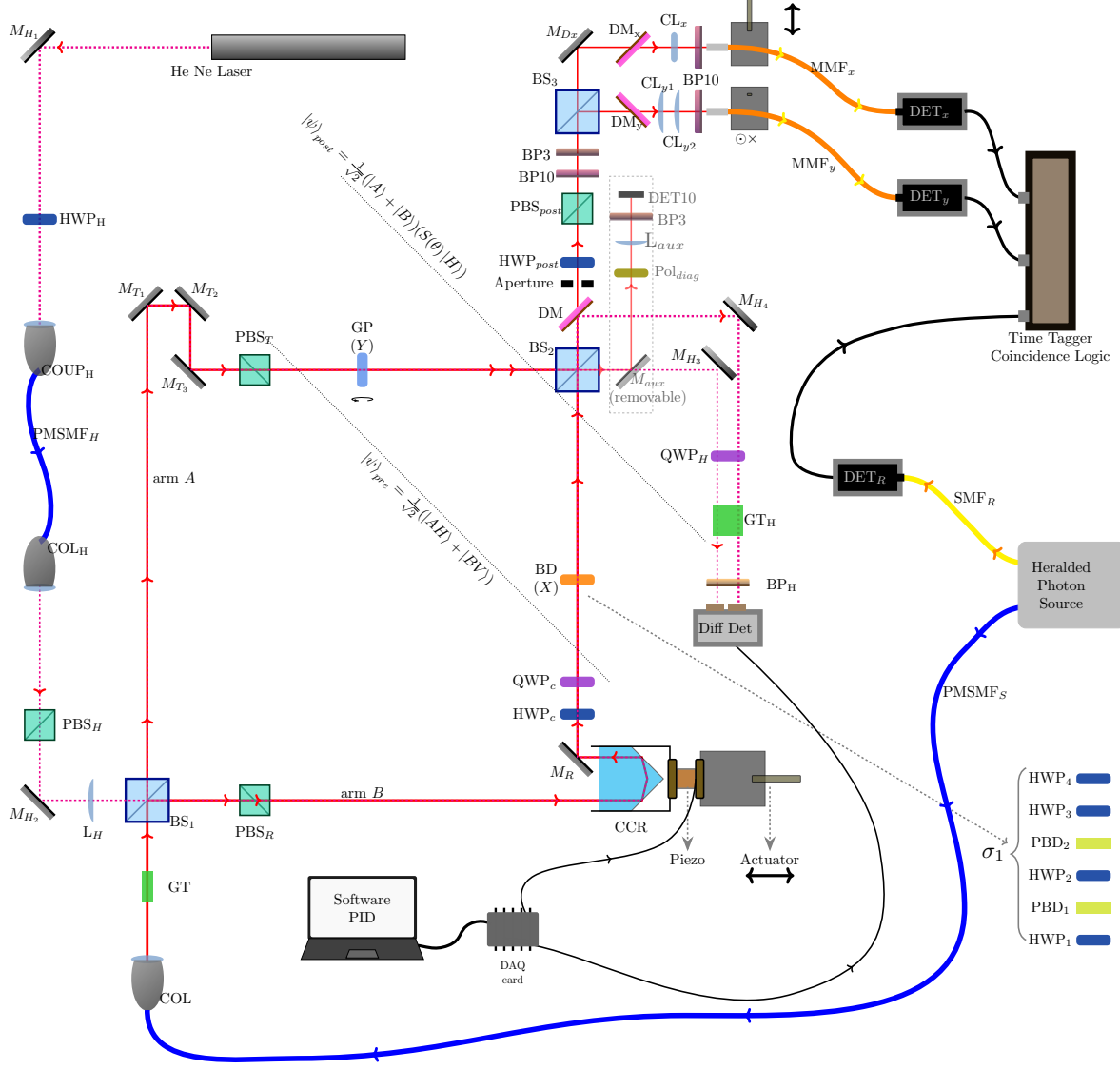


FIG. A-1: Experimental setup

voltages. The phase shift in the interferometer is monitored by measuring the difference in power in the two output ports of the second beam splitter BS_2 for a Helium Neon (He Ne) beam of wavelength 633 nm, inserted into the MZI from the other input port of the first beam splitter (BS_1). This beam is mostly blocked by the Dichroic Mirror DM [DMLP735, Thorlabs] placed after BS_2 in addition to the band pass filters (BP10 and BP3). Before the differential detector (Diff Det), the polarizations of the He Ne beams coming from two output ports of BS_2 are transformed into circular basis using quarter-wave plate QWP_H and then projected to horizontal polarization using GT_H to achieve maximum visibility. The differential intensity signal obtained from the 633 nm beam is

calibrated with the intensity of the 810 nm laser measured at the other output port (at which the post selection is not performed) of BS_2 with diagonal polarization projection using photodetector [DET10/M, Thorlabs] as a function of voltage given to the piezoelectric transducer. When the path difference is within one wavelength, these two signals become almost linear enabling the usage of the differential intensity signal to stabilize the phase difference within low uncertainty.

Weakly coupling the spatial DOF using a tilted glass plate

A parallel window GP [WG41010-B, Thorlabs] is placed in arm A and is tilted to cause a vertical shift of ~ 50 microns in the beam. Tuning the angle of tilt of the glass plate, the shift in the beam can be controlled. If the shift were more than the beam width of 1.9 mm, observing this shift after the post-selection would have indicated whether the photon came from arm A or arm B. The shift of ~ 50 microns being much less than the beam width ensures that the observable (\hat{Y}_A) is weakly coupled.

Weakly coupling the diagonal component of polarisation DOF using a composite beam displacer

A polarising beam displacer (PBD) allows the ordinary component of polarization of the beam incident on it to pass through without any deviation and causes a lateral shift (depending upon its thickness) in the path of the extraordinary component of polarization of the incident beam. Thus, the operation of a PBD can be considered as σ_3 measurement operation. The σ_1 measurement operator can be constructed from the σ_3 measurement operation. Here the σ_3 measurement operator is created using two beam displacers PBD_1 and PBD_2 [PDC 12005, Newlight Photonics] oriented in such a way that one of them causes ~ 50 microns shift in the extraordinary component along one direction (say +X) and the other shifts the extraordinary component by ~ 50 microns in the opposite direction (-X) horizontally. A half wave plate HWP_2 (fast axis at $\pi/4$) is inserted between the two beam displacers so that the extra-ordinary beam for the first PBD becomes the ordinary component for the second PBD and vice versa. This is followed by another half wave plate HWP_3 (with fast axis at $\pi/4$) so that the ordinary and the extra-ordinary polarized beams have the same phase in the description of the σ_3 operator. The whole σ_3 measurement operator is placed between two half wave plates HWP_1 and HWP_4 [WPA03-H-810] with their fast axes oriented at angle $\pi/8$ to realise the σ_1 operator.

Alignment procedure for joint observation

Ideally, the zero reference of the beam, on a 2D plane after the post-selection would be at the position where both the beams from arm A and arm B merge. They are expected to be overlapping and collinear at the detection plane. However, when components for the weak interaction with the σ_1 polarization component are inserted in arm B, the beam displacers (PBD_1 and PBD_2) need to be tilted in order to adjust the phase shift between the emergent e-ray and o-ray so that in the limit of the beam displacement between them going to zero, the evolution operator due to the interaction remains identity. Due to the tilt as well as a slight angular deviation of the beam from components, the beam in arm B gets refracted after the components are inserted. This causes a slight non-collinearity and translation of the beam. The change in collinearity is very small and can be adjusted by maximizing the visibility when post selection is either diagonal or anti-diagonal. This is achieved by the tip/tilt of the mirror M_R . The displacement between the diagonal and anti-diagonal components is fixed by the alignment in components (PBD_1 and PBD_2) for the σ_1 interaction. However, they should ideally be on either side, equidistant from the centre of the beam emerging from arm A. One way to verify this would be to measure the beam centre position from arm A with arm B blocked and vice versa. However, when arm A is blocked, the pre-selected polarization in arm B is orthogonal to the post-selected polarization. Due to the displacement between diagonal and anti-diagonal components, we have the destructive interference pattern after post-selection as shown in Figure A-2.

The centroid of the destructive interference pattern tends to be error prone. Therefore, utilising the fact that the centres of the beams in arms A and arm B coincide, one needs to use the resultant interference pattern formed when the post-selection is diagonal and anti-diagonal. From theory, these two displacements need to be symmetric about the centre of the beam of arm A. This is achieved by translating the CCR and measuring the resultant centroid at three post-selection configurations. Once the above alignment is ensured, the glass plate in arm A which was back aligned, is now tilted so that it causes the desired shift along the vertical direction when arm B is blocked. All the above steps are performed with pulsed laser and data is acquired with a beam profiler. The 2D centroid of the beam is scaled to the weak value. The scaling can be achieved by subtracting the ensured zero position as mentioned earlier and scaling it with the pointer shift corresponding to the eigenvalues with individual arms blocked. This can be done with beam profiler data as blocking and insertion of components are all performed with beam profiler as the monitoring tool for

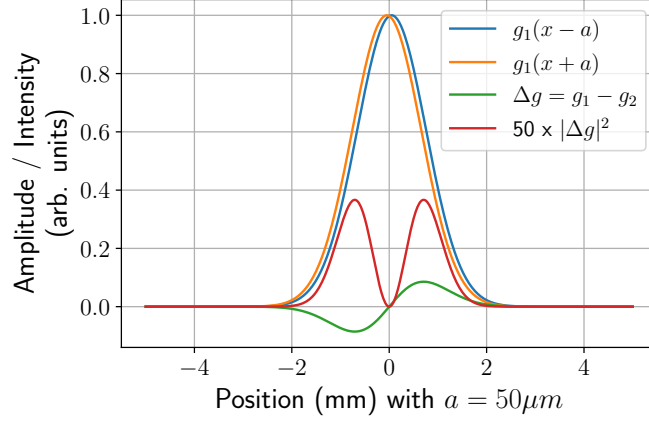


FIG. A-2: Destructive Interference intensity pattern (shown after multiplication by 50 in red) is obtained when two Gaussians g_1 and g_2 are displaced in opposite direction by the displacement a . The centroid of this interference pattern has more error due to the presence of noise. The centroid of the pattern is also very sensitive to the phase difference between the two Gaussian beams.

the pulsed laser source. However, once the measuring device is changed, the information about absolute position in different configurations is lost. The beam profiler is then taken out of the setup and the multimode fibres mounted on a translation stage are used. The weak value is measured at the three post-selection angles to ensure that the alignment of multi-mode fibres is consistent with the beam profiler data. Once the above is ensured, the pulsed laser beam is replaced with stream of single photons coming from a single photon source to measure singles and coincidences. Here, we scale the pointer shift to weak values by subtracting the pointer shift at post-selection HWP angle 45° (corresponding to the zero weak value). Similarly, displacement by weak value 1 happens when post-selection HWP angle is 90° .

2. Results

Data Acquisition

In order to subsequently use a single photon source, a 100 fs pulsed laser [Mira 900 D Ti:Sapphire, rep rate: 76 MHz] is used with average power of about 2 mW to ensure good alignment. Although the coherence length of the pulsed laser is lower (than CW), it is slightly enhanced by the use of the bandpass filter so that the pulsed laser has almost the same central

wavelength and the bandwidth as the single photon source to be used later. A beam profiler [Dataray UCD -15] is placed after the bandpass filter. The post-selection HWP angle is rotated to the angle 67.5° that creates the destructive interference profile along the diagonal. The phase difference is adjusted to make this destructive interference pattern as symmetric as possible along the diagonal. The slight spatial noise in the beam profile i.e., deviation from a perfect Gaussian profile typically would dominate the destructive interference pattern. The overall power incident on the beam profiler also reaches the minimum which is another indicator for the correct phase difference to which the Mach Zehnder interferometer is locked. The post selection HWP angle is rotated and 5 images are captured for each HWP angle. The first order centroid of the 2D images is computed. The pointer shifts are scaled to the weak value using the pointer shifts at 45° and 90° as reference.

For the single photon source, the timing information along with the spatial profile needs to be measured. The timing information ensures that the contribution of multi-photon events to the pointer shift is negligible. For this SPAD detectors [Tau SPAD-20, Pico quant] are used. The photons are collected using a bare multimode fibre [M42L02, Thorlabs] with a core diameter of 50 microns. These fibres (MMF_x and MMF_y) are moved in steps of 50 microns to sample the Gaussian profile. A width of about 3 mm is covered with 61 points. Although the use of such fibres averages the intensity over the 50 microns, the precision with the centroid is much better than this and depends on the total number of photons collected. To enhance the collection, a (combination of) cylindrical lens (CL_x , CL_{y_1} and CL_{y_2}) is used to compress one spatial dimension. The multi-mode fibre tip is placed at the focus of the cylindrical lens and is translated to obtain the spatial profile.

Since the objective is to jointly observe the two pointers, a 50:50 beam splitter BS_3 [BS014] is used to divide the beam. One beam is used to reconstruct the horizontal profile (X) and the other beam is used to reconstruct the vertical profile (Y). Since the beam splitter sends the photon towards the horizontal or the vertical detector with inherent randomness and there is no change of experimental settings within the interferometer (i.e., between pre and post-selection), the horizontal and vertical centres of the beam are jointly obtained for the ensemble of photons for a given post-selected state.

Statistics and Error Analysis

When the post selection HWP angle is set to 0° , 16 coincidence readings per position of the MMF are taken. Any one of these 16 readings at a particular position is chosen and it

is repeated for all the 61 positions to construct a Gaussian profile. Thus 16^{61} such possible profiles can be constructed from the collected data. Out of that, 10^4 such Gaussian profiles are sampled and each such profile is fitted with a Gaussian function to determine the centre. This gives the distribution of the position of the pointer (say X) for the post-selected state $|\phi\rangle$ (when the HP_{post} angle is at 0°).

Let us call the distribution of centres when the post-selection angle is 45° as X_0 . The 10^4 profiles for this post-selected state $|\phi(45^\circ)\rangle$ are sampled from datasets with 3 readings for each MMF position (amounting to 3^{61} possible profiles).

Similarly, we have 3 readings per MMF position at the post-selection angle 90° . The corresponding distribution of centres of the beam for the post selected state $|\phi(90^\circ)\rangle$ is, say X_1 , which again is obtained from Gaussian fits of 10^4 profiles.

Since the profiles are drawn at random, we can create the distribution of weak values by computing,

$$X^w = \frac{X - X_0}{\langle X_1 - X_0 \rangle}$$

The statistical random errors are represented by standard deviation of X^w . The random errors come from the numerator since we have taken the expectation value in the denominator. This is to avoid spurious weak values if some of the values in the denominator turn out to be zero by chance.

On measuring few profiles at a particular post-selection angle and then changing the post-selection angle to observe a certain shift, it could so happen that the observed shift is more or less than expected due to drift in the position of the beam over time. This drift typically arises from the effect of temperature, pressure and humidity on opto-mechanics and fibres (mainly $PMSMF_s$). The beam drift is estimated in a separate experiment where the transverse profile of the beam in arm A (with arm B blocked) is repeatedly measured with the moving MMF for a long period. The drift in centroid would represent the drift of the beam's centre over time. The standard deviation of the centroid over time indicates the range of the systematic error which changes the unit scale of the weak value.

Single Photon Source Characteristics

The experiment uses a heralded single photon source generated using spontaneous parametric down-conversion of 405 nm pump beam in a type-II PPKTP crystal in a collinear Sagnac geometry. As shown in Figure A-1 one stream of photons (signal photons) is made

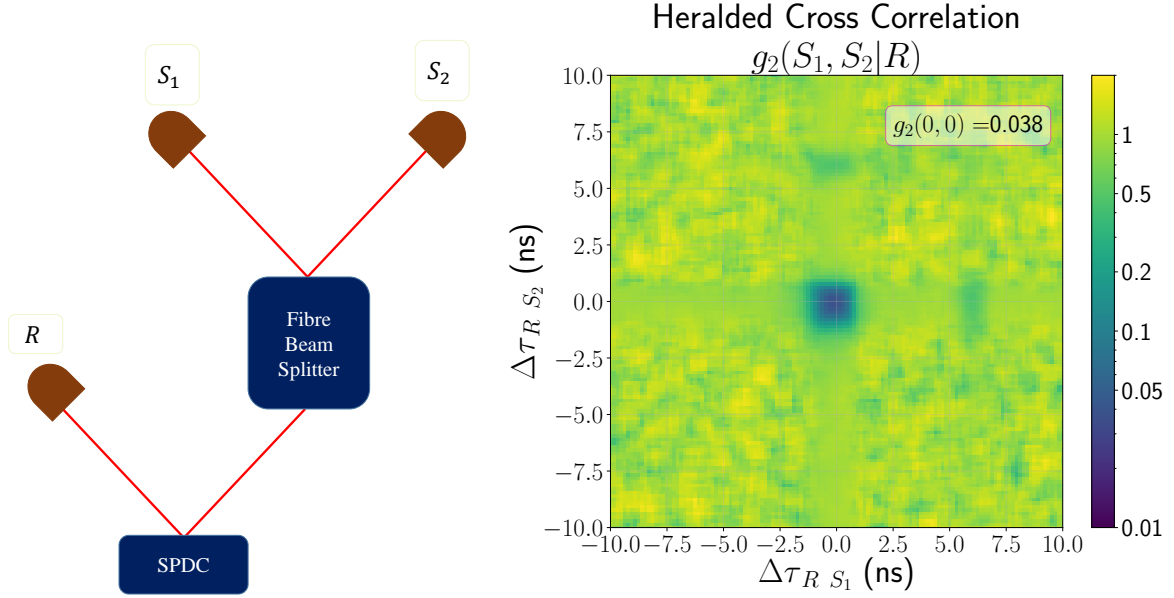


FIG. A-3: Heralded cross correlation (pump power 20 mW, coincidence time window 312.5 ps).

incident on the MZI using a polarization maintaining single-mode fibre ($PMSMF_S$). Although the source is bright and singles count rate is in the MHz domain, photons with rates in the kHz domain are detected with the multi-mode fibres (MMF_x, MMF_y shown in Figure A-1 due to the collection area of the fibres. Each stream of photons (singles) is known to have Poissonian statistics and only the heralded photons (coincidences) follow sub-Poissonian statistics. The heralded cross-correlation function is defined for the SPDC process as

$$g_2(\Delta\tau_1, \Delta\tau_2) = \frac{N(R)C(S_1(\Delta\tau_1), S_2(\Delta\tau_2)|R)}{C(S_1(\Delta\tau_1)|R)C(S_2(\Delta\tau_2)|R)}.$$

Here, $N(R)$ is the number of photons in the reference (R) detector DET_R in a given time duration (see Figure A-3). $C(S_1(\Delta\tau_1), S_2(\Delta\tau_2)|R)$ refers to the triple coincidences when S_1 is delayed by $\Delta\tau_1(= \Delta\tau_{RS_1})$ and S_2 is delayed by $\Delta\tau_2(= \Delta\tau_{RS_2})$ with respect to R . The coincidences between R with S_1 delayed by $\Delta\tau_1$ and between R with S_2 delayed by $\Delta\tau_2$ is denoted by $C(S_1(\Delta\tau_1)|R)$ and $C(S_2(\Delta\tau_2)|R)$ respectively.

The $g_2(0,0)$ is about 0.038 thus implying that the stream of photons from S_1 or S_2 when heralded with R shows single-photon characteristics.

Appendix B: Theoretical details

1. Standard intermediate measurements in the Mach-Zehnder interferometer

a. Setting

We consider the Mach-Zehnder interferometer given in the main text and derive the probabilities for strong intermediate measurements along the arms A and B . The pre and post-selected states were given respectively by

$$|\psi\rangle = \frac{1}{\sqrt{2}} (|A\rangle |H\rangle + |B\rangle |V\rangle) \quad (\text{B1})$$

and

$$|\phi\rangle = \frac{1}{\sqrt{2}} (|A\rangle + |B\rangle) |H\rangle. \quad (\text{B2})$$

$\langle r|A\rangle$ and $\langle r|B\rangle$ are the spatial wavefunctions of the photon along arms A and B (r is the position), while $|H\rangle$ and $|V\rangle$ correspond to horizontal and vertical polarization.

The properties we are interested in are:

- the spatial projectors on arms A and B, represented by the observables $\hat{Y}_A = |A\rangle\langle A| \otimes \hat{\mathbb{I}}$ and $\hat{Y}_B = |B\rangle\langle B| \otimes \hat{\mathbb{I}}$, having eigenvalues $Y_i = 0, 1$ ($i = A, B$); note that

$$\hat{Y}_A + \hat{Y}_B = \mathbb{I}, \quad (\text{B3})$$

so that a positive measurement of \hat{Y}_A (with eigenvalue $Y_A = 1$) is also a negative measurement of \hat{Y}_B (with eigenvalue 0).

- the diagonal polarization of the photon on each arm, represented by the observables $\hat{X}_A = |A\rangle\langle A| \otimes \sigma_1$ and $\hat{X}_B = |B\rangle\langle B| \otimes \sigma_1$ where σ_1 is one of the Pauli matrices with eigenstates

$$|\nearrow\rangle = \frac{1}{\sqrt{2}} (|H\rangle + |V\rangle) \quad (\text{B4})$$

$$|\searrow\rangle = \frac{1}{\sqrt{2}} (|H\rangle - |V\rangle). \quad (\text{B5})$$

$|\nearrow\rangle$ and $|\searrow\rangle$ correspond to diagonal and anti-diagonal polarization. The eigenvalues of \hat{X}_i are $X_i = -1, 1$ and 0 (corresponding respectively to anti-diagonal, diagonal and no polarization on arm i).

b. Spatial degree of freedom

Let us first consider a non-destructive measurement of the spatial wavefunction when the photon is prepared in state $|\psi\rangle$. If we measure the spatial degree of freedom on arm A, the state after the intermediate measurement is projected to $\hat{Y}_A |\psi\rangle = |A\rangle |H\rangle$ if the measurement is successful ($Y_A = 1$). This happens with a probability

$$P(Y_A = 1) = \text{Tr}_Y \hat{Y}_A \text{Tr}_X |\psi\rangle \langle \psi| = \frac{1}{2}. \quad (\text{B6})$$

The probability of post-selection after this successful measurement is then

$$P(|\phi\rangle | Y_A = 1) = |\langle \phi | A \rangle | H \rangle|^2 = \frac{1}{2}. \quad (\text{B7})$$

Since $P(\phi) = |\langle \phi | \psi \rangle|^2 = 1/4$, following Bayes' theorem the conditional probability of finding the particle's spatial degree of freedom on arm A when post-selection is succesful is [1]

$$P(Y_A = 1 | \phi) = 1. \quad (\text{B8})$$

Given Eq. (B3), the conditional probability of finding the position degree of freedom on arm B given post-selection is therefore

$$P(Y_B = 1 | \phi) = 0. \quad (\text{B9})$$

This can also be seen from the direct computation of $P(|\phi\rangle | Y_B = 1) = |\langle \phi | B \rangle | V \rangle|^2 = 0$.

Let us introduce a pointer on arm A in state $|\xi_{x_0}\rangle_A$; its wavefunction is $\langle x | \xi_{x_0} \rangle_A = \xi_{x_0}(x)$, where x_0 is the mean initial position of the pointer. Assume the usual von-Neumann type coupling

$$H_{int} = \gamma(t) \hat{Y}_A \hat{P} \quad (\text{B10})$$

between the pointer's momentum \hat{P} and the particle observable \hat{Y}_A . $\gamma(t)$ is the coupling strength and let $g = \int \gamma(t) dt$ label the overall coupling strength taken over the interaction time. g is chosen such that the shifted pointer state $|\xi_{x_0+g}\rangle_A$ is orthogonal to the initial state, i.e. ${}_A \langle \xi_{x_0+g} | \xi_{x_0} \rangle_A = 0$. Unitary evolution brings the initial state

$$|\Psi(t_i)\rangle = |\psi\rangle |\xi_{x_0}\rangle_A \quad (\text{B11})$$

to the time evolved state after the interaction

$$|\Psi(t)\rangle = e^{-ig\hat{Y}_A\hat{P}/\hbar} |\psi\rangle |\xi_{x_0}\rangle_A \quad (\text{B12})$$

$$= \frac{1}{\sqrt{2}} (|A\rangle |H\rangle |\xi_{x_0+g}\rangle_A + |B\rangle |V\rangle |\xi_{x_0}\rangle_A), \quad (\text{B13})$$

where we have used the translation property of the operator $e^{-ig\hat{Y}_A\hat{P}/\hbar}$. Postselecting the system to state $|\phi\rangle$ [Eq.(B2)] leaves the pointer in the shifted state $|\xi_{x_0+g}\rangle$. This indicates that the postselected photon has traveled through arm A. Similarly, we can place a pointer on arm B, in the initial state $|\xi_{x_0}\rangle_B$. Eq. (B13) is then replaced by

$$\frac{1}{\sqrt{2}} (|A\rangle |H\rangle |\xi_{x_0}\rangle_B + |B\rangle |V\rangle |\xi_{x_0+g}\rangle_B) \quad (\text{B14})$$

After post-selection to state $|\phi\rangle$, the pointer will be found in its initial state $|\xi_{x_0}\rangle_B$ (since the term $|B\rangle |V\rangle |\xi_{x_0+g}\rangle_B$ is orthogonal to the post-selected state): there is no displacement of the pointer, indicating that the postselected photon has not traveled through arm B.

The conclusion is that a standard non-destructive intermediate measurement of the spatial degree of freedom with pre and post-selection states given by Eqs. (B1) and (B2) will always result in a pointer shift on arm A, while the pointer on arm B remains in the initial (unshifted) state.

c. Diagonal polarization degree of freedom

While an intermediate measurement of the spatial degree of freedom (DOF) is only detected on arm A, it is easy to see that measuring the diagonal polarization DOF on arm B can result in detecting $|\nearrow\rangle$ or $|\searrow\rangle$ with a probability given by

$$P(X_B = \pm 1|\phi) = \frac{1}{4}. \quad (\text{B15})$$

So although the spatial DOF is never detected on arm B, a different property, namely the diagonal component of the polarization DOF will be detected there half of the runs. A pointer's momentum can be coupled to the diagonal polarization observable σ_1 on arm A or B, similarly to the spatial projection operator case (B12) (with now two shifted states $|\xi_{x_0\pm g}\rangle$ corresponding to $X_i = \pm 1$).

It is also possible to couple a qubit pointer to the diagonal polarisation of the photon on a given arm, so that the interaction Hamiltonian reads $H_{int} = \gamma(t)\sigma_1\sigma_2^g$ where σ_2^g is a Pauli matrix relevant to the qubit pointer and $g = \int \gamma(t)dt$ can be chosen so that the initial qubit state $|0_g\rangle$ is rotated conveniently. Such a qubit pointer will only be excited when

placed in arm B, as we will see below. Let us first examine the qubit behaviour after it gets coupled to the system through H_{int} . Consider a polarized state in the diagonal basis given by $|\chi\rangle = \alpha |\nearrow\rangle + \beta |\searrow\rangle$ with α, β assumed to be real (a generalization for any point on the Bloch sphere is possible but will not be needed here). Let us introduce the quantity $|\alpha - \beta|^2$ that we may call the “net diagonal polarization”. Let $|0_q\rangle$ denote the ground state of the qubit pointer. The photon and qubit evolve from $|\chi\rangle |0_q\rangle$ to

$$e^{-ig\sigma_1\sigma_2^q} |\chi\rangle |0_q\rangle \quad (\text{B16})$$

$$= \left(e^{-ig\sigma_2^q} \alpha |\nearrow\rangle + e^{ig\sigma_2^q} \beta |\searrow\rangle \right) |0_q\rangle \quad (\text{B17})$$

$$= \alpha |\nearrow\rangle (\cos g |0_q\rangle + \sin g |1_q\rangle) + \beta |\searrow\rangle (\cos g |0_q\rangle - \sin g |1_q\rangle) \quad (\text{B18})$$

$$= \cos g (\alpha |\nearrow\rangle + \beta |\searrow\rangle) |0_q\rangle + \sin g (\alpha |\nearrow\rangle - \beta |\searrow\rangle) |1_q\rangle. \quad (\text{B19})$$

If the polarization is then measured in the linear basis and post-selected in state $|H\rangle$, the qubit is left in state

$$(\alpha + \beta) |0_q\rangle \cos g + (\alpha - \beta) |1_q\rangle \sin g. \quad (\text{B20})$$

For definiteness let us set $g = \pi/4$. If $|\chi\rangle = |H\rangle$, the net diagonal polarization is 0 and the qubit detector remains in its ground state. For $|\chi\rangle = |V\rangle$ the detector is found with unit probability in the excited state.

Now in a Mach-Zehnder set-up, if we place a qubit pointer in state $|0_q\rangle_A$ in arm A and apply $H_{int} = \gamma(t)\hat{X}_A\sigma_2^q$ the evolution of the joint system-pointer state can be given as (keeping $g = \pi/4$)

$$e^{-ig\hat{X}_A\sigma_2^q} |A\rangle |H\rangle |0_q\rangle_A + |B\rangle |V\rangle |0_q\rangle_A \quad (\text{B21})$$

$$= \frac{1}{\sqrt{2}} (|A\rangle |H\rangle |0_q\rangle_A + |A\rangle |V\rangle |1_q\rangle_A) + |B\rangle |V\rangle |0_q\rangle_A \quad (\text{B22})$$

Postselecting to $|\phi\rangle$ [Eq. (B2)] leaves the pointer in the ground state $|0_q\rangle_A$ with unit probability. Similarly, a qubit pointer in arm B coupled through $H_{int} = \gamma(t)\hat{X}_B\sigma_2^q$ leads to the evolved state $(|B\rangle |V\rangle |0_q\rangle_B + |B\rangle |H\rangle |1_q\rangle_B) / \sqrt{2} + |A\rangle |H\rangle |0_q\rangle_B$. The term $|B\rangle |H\rangle |1_q\rangle_B$ is compatible with postselection, so the qubit pointer can be found in the excited state $|1_q\rangle_B$ with a non-zero probability.

d. Disturbing joint measurement

Let us finally consider the joint intermediate measurement of the spatial DOF on arm A (\hat{Y}_A) and of the diagonal polarization DOF on arm B (\hat{X}_B) via coupling Hamiltonians $g\hat{Y}_A\hat{P}_y$ and $g\hat{X}_B\hat{P}_x$ respectively, where \hat{P}_y (\hat{P}_x) refers to the momentum of the pointer in arm A (arm B). Let $|\xi_{y_0}\rangle$ and $|\xi_{x_0}\rangle$ denote the initial states of the pointer in arm A and arm B respectively. The evolution of the joint system-pointer state can be written as

$$|\Psi(t)\rangle = e^{-ig\hat{Y}_A\hat{P}_y/\hbar} e^{-ig\hat{X}_B\hat{P}_x/\hbar} |\psi\rangle |\xi_{y_0}\rangle |\xi_{x_0}\rangle \quad (\text{B23})$$

$$= \frac{1}{\sqrt{2}} |A\rangle |H\rangle |\xi_{y_0+g}\rangle |\xi_{x_0}\rangle + \frac{1}{2} |B\rangle |\xi_{y_0}\rangle (|\nearrow\rangle |\xi_{x_0+g}\rangle - |\searrow\rangle |\xi_{x_0-g}\rangle). \quad (\text{B24})$$

After post-selecting to state (B2) (and assuming the shifted pointer states are orthogonal to their initial states) we will either find the pointer coupled to the spatial DOF on arm A shifted by an amount g along the y axis and the pointer on arm B coupled to the diagonal polarization DOF unshifted; or we will find that the pointer on arm B has shifted by $\pm g$, while the pointer on arm A remains unshifted.

Summing up the different cases we have considered concerning measurements at an intermediate time inside the interferometer, we therefore see that:

- If only the spatial DOF is measured, the photon is always found on path A, never on arm B.
- If the diagonal polarization DOF is measured then it will be found in arm B with a non-zero probability. If the diagonal polarization DOF is coupled to a qubit detector, such a detector will never be triggered in arm A.
- If the spatial and the diagonal polarization DOFs are measured on paths A and B respectively, the photon (as measured by its spatial degree of freedom) is found on path A only half of the times. The other half, the photon's diagonal polarization measurement is successful on path B, with the pointer on arm B shifting in either the positive or negative directions.

Of course, these statements refer to three different setups. Quantum measurements disturb the entire setup comprising the photon and the measurement devices. It is not possible (except in a counterfactual sense) to make any statement on a property of the photon that

was not measured. Indeed, these statements do not hold for the same photon, but for distinct particles moving inside an inteferometer with distinct experimental arrangements.

2. Weak measurements and weak values in the Mach-Zehnder interferometer

a. Weak values

We consider the same Mach-Zehnder interferometer and pre and post selected states $|\psi\rangle$ and $|\phi\rangle$ given above [see Eqs. (B1) and (B2)]. An intermediate weak measurement involves the same type of von Neumann interaction that was given above for strong measurements [see Eq.(B12)] in a pre/post-selected context. More precisely, let \hat{S} denote the system observable and assume a system-pointer interaction $H_{int} = \gamma(t)\hat{S}\hat{P}$ coupling \hat{S} to \hat{P} (the momentum of the pointer). The ensuing unitary evolution operator $\exp(-i \int H(t')dt'/\hbar)$ brings the initial state $|\Psi(t_i)\rangle = |\psi\rangle |\xi_{x_0}\rangle$ to

$$|\Psi(t)\rangle = e^{-ig\hat{S}\hat{P}/\hbar} |\psi\rangle |\xi_{x_0}\rangle \quad (\text{B25})$$

$$\simeq \left(I - ig\hat{S}\hat{P}/\hbar \right) |\psi\rangle |\xi_{x_0}\rangle \quad (\text{B26})$$

where $|\xi_{x_0}\rangle$ is the unshifted initial pointer state and $g = \int \gamma(t)dt$ is now considered to be small so that the first order asymptotic expansion holds. Actually more stringent conditions need to hold [2], involving a sufficient width of the pointer state and the transition amplitudes of \hat{S} . Successful post-selection implies the projector $\Pi_\phi = |\phi\rangle \langle\phi|$ is applied to the system state. The system-pointer state after post-selection becomes

$$|\phi\rangle \langle\phi| \psi\rangle \exp\left(-igS^w\hat{P}/\hbar\right) |\xi_{x_0}\rangle, \quad (\text{B27})$$

$$= \nu \langle\phi| \psi\rangle |\phi\rangle |\xi_{x_0+g\text{Re}(S^w)}\rangle, \quad (\text{B28})$$

where we have re-exponentiated the term

$$S^w = \frac{\langle\phi|\hat{S}|\psi\rangle}{\langle\phi|\psi\rangle} \quad (\text{B29})$$

known as the *weak value* [3] of \hat{S} given the pre and post-selected states $|\psi\rangle$ and $|\phi\rangle$. ν is a normalization constant.

In general S^w is a complex number. Since $\exp(-ia\hat{P})$ with a real is a translation operator, the pointer is shifted by $g\text{Re}(S^w)$. The shift is small (relative to the pointer width) implying

enough statistics must be gathered in order to observe the shift position with low uncertainty. Note this shift is the result of the interaction of the pointer momentum with the system observable, and of the post-selection. When $\text{Re}(S^w) = 0$, the pointer does not shift despite the coupling interaction. Operationally the property represented by \hat{S} is not recorded by the pointer when the system is post-selected. This can be interpreted [4] as the absence, at the location of the pointer, of the property corresponding to the coupled system observable. The imaginary part $\text{Im } S^w$ is interesting in its own right [5], but in the present context it plays no role and we simply include it in the normalization constant ν .

b. Joint weak values of the spatial and diagonal polarization degrees of freedom

Given our pre and post-selected states, it is straightforward to apply Eq. (B29) to \hat{Y}_A . This yields the weak value of the spatial projector on path A,

$$Y_A^w = \frac{\langle \phi | \hat{Y}_A | \psi \rangle}{\langle \phi | \psi \rangle} \quad (\text{B30})$$

$$= \langle A | \langle H | A \rangle | H \rangle \quad (\text{B31})$$

$$= 1. \quad (\text{B32})$$

Y_B^w is not independent from Y_A^w , since by Eq. (B3) we must have for any pre and post-selected states

$$Y_A^w + Y_B^w = \frac{\langle \phi | \psi \rangle}{\langle \phi | \psi \rangle} = 1. \quad (\text{B33})$$

Therefore $Y_B^w = 0$ holds algebraically by virtue of Eq. (B3).

For the diagonal polarization $\hat{X}_i = |i\rangle \langle i| \otimes \sigma_1$, we have on path B

$$X_B^w = \frac{\langle \phi | \hat{X}_B | \psi \rangle}{\langle \phi | \psi \rangle} \quad (\text{B34})$$

$$= \langle B | \langle H | \sigma_1 | B \rangle | V \rangle \quad (\text{B35})$$

$$= 1. \quad (\text{B36})$$

X_A^w is not independent from X_B^w , since

$$X_A^w + X_B^w = \frac{\langle \phi | \sigma_1 | \psi \rangle}{\langle \phi | \psi \rangle} \quad (\text{B37})$$

$$= 1, \quad (\text{B38})$$

where the last equality is state-dependent and holds for our specific choices of pre and post-selected states, leading to $X_A^w = 0$.

The upshot is that

$$Y_A^w = 1 \Rightarrow Y_B^w = 1 - Y_A^w = 0 \quad (\text{B39})$$

$$X_B^w = 1 \Rightarrow X_A^w = 1 - X_B^w = 0. \quad (\text{B40})$$

It is therefore necessary to measure jointly only the two weak values Y_A^w and X_B^w on the same photon in order to observe conclusively the separation between the spatial degree of freedom on path A, and the diagonal polarization degree of freedom on path B.

-
- [1] These conditional probabilities are known as the ABL rule, see Y. Aharonov, P. G. Bergmann and J. L. Lebowitz, Phys. Rev. B 134, 1410 (1964).
 - [2] See e.g. I. M. Duck, P. M. Stevenson, and E. C. G. Sudarshan, Phys. Rev. D 40, 2112, 1989.
 - [3] The weak value was introduced in Y. Aharonov, D. Z. Albert, and L. Vaidman, Phys. Rev. Lett. 60, 1351 (1988).
 - [4] See A. Matzkin, Found. Phys. 49, 298?316 (2019) and Refs. therein.
 - [5] See J. Dressel and A. N. Jordan, Phys. Rev. A 85, 012107 (2012).